Laser micro annealing conditioning for the suppression of statistical scatter in freestanding Sb_2Te_3 nanowire resistance

M. Mikulics[a,b*], J. G. Lu[c], L. Huang[c], P. L. Tse[c], J. Z. Zhang[d], J. Mayer[a,b] and H. H. Hardtdegen[a,b*]

[a]*Ernst Ruska-Centre (ER-C-2), Forschungszentrum Jülich, D-52425 Jülich, Germany*

[b]*Jülich Aachen Research Alliance Fundamentals of Future Information Technology (JARA-FIT)*

[c]*Department of Physics and Department of Electrical Engineering, University of Southern California, Los Angeles, California, USA*

[d]*Department of Electronic Engineering, East China Normal University, Shanghai, 200241, China*

Keywords: correlative studies, laser annealing, local contact formation, hybrid nanodevice, nanowire photodetector

Abstract

The effect of long-term laser micro annealing (LMA) on the statistical resistance scatter in freestanding Sb_2Te_3 layered nanowires (NWs) was studied during the formation of ohmic contacts. The process was developed and optimized by monitoring the evolution of the NW resistance and the DC photo-responsivity and correlating the characteristics to the structural degradation observed using micro Raman spectroscopy. The NWs were transferred to and integrated into Ti/Au coplanar strip lines on flexible polyethylene terephthalate (PET) substrates designed for optoelectronic applications. Four different stages in the NWs´ resistance were revealed. The optimal "time-annealing" interval was identified, in which the lowest NW resistance was determined and in which no evidence for structural degradation processes in the active central NWs´ region was found. Low dark currents below 10^{-5}A at 100 mV bias as well as high DC photo-responsivity ~ 0.6 A/W were achieved rendering the nanowire devices as very promising candidates for highly sensitive infrared optoelectronics. The statistical scatter in the NWs´ resistance was minimized to a range of ±10% of the total value by conditioning the contact/annealed regions of the NWs individually and tuning the resistance of these regions as a function of the total laser annealing time.

*E-mail: m.mikulics@fz-juelich.de
*E-mail: h.hardtdegen@fz-juelich.de

1. Introduction

Currently there is a growing interest in low dimensional chalcogenide layered structures and the disclosure of future applications [1-4]. To this end, also alternative device concepts implementing different classes of materials and different dimensionalities within hybrid nano-optoelectronic devices [5-12] may play a large role in their applications. The small dimensions of such nanostructures are advantageous for obtaining a high integration density on the one hand and for the utilization of quantum size effects on the other hand [13-15]. Furthermore, nanostructures exhibiting different physical, chemical, optical and electrical properties could be combined into hybrid circuits for novel nanostructure devices with enhanced functionality if a suitable and efficient nanostructure transfer and integration technology were available [12]. However, nano-scaled objects are extremely sensitive to handle and to integrate into device circuits due to the ease of their deterioration during the processing technology. This is especially the case for materials in the family of layered chalcogenide structures.

The spatial and temporal control for processing and material modification using lasers as the energy sources emerged as a new field in material science in the late 1970`s. Laser annealing was employed for example to heal ion implantation damage [16-18] and lately in the processing of nanostructures and especially in the annealing of contacts to nanostructures [19-22]. In general, the aim of these latter studies was to reduce the contact resistance and – for practical and industrial applications – to use as small as possible annealing times. In contrast, the idea behind our long-term annealing procedure concerns the systematic study and the evolution, observation as well as monitoring of the nanowire resistance and the structural changes. In this way, it would be possible to understand the complex and characteristic features of annealing on contact formation. Furthermore, the characteristics of nanostructures tend to be subject to a large statistical scatter. This was, however, not in the center of attention up to now. The scatter is initialized for example by fluctuations of the growth conditions locally or over the large substrate´s area and/or by lithographical and technological imperfections. Explicitly nanowires (NWs) exhibit a large statistical scatter with respect to their conductance/resistance. However, it is a crucial point for the integration of a large number of individual nanowires in highly sophisticated integrated circuits that the parameters of each individual nanowire based device should be close to an “average” value for all single computational units. Then, optimal charge transport, homogeneous heat development as well as time synchronization in the circuit is ensured especially for those designated for future quantum-, cryptography- computational techniques. Therefore, there is a strong need for

suitable and simple techniques to compensate for scatter in the NWs´ resistance and to ideally tune device parameters close to/into the range designed for operation. Ideally, the technique should not alter the material characteristics of the nanostructure itself.

In this report Sb_2Te_3 layered NWs were studied. Our Sb_2Te_3 NWs were transferred directly after growth from their native ”mother” substrate to the “host” flexible polyethylene terephthalate (PET) substrate containing coplanar strip lines and integrated using NW transfer and integration techniques [23-25]. By doing so, possible technological and chemical influences of photo and/or e-beam lithography, their resists and or developers are avoided. The NWs were bonded to the strip lines by van der Waals forces. A suitable and simple technique was developed for this highly sensitive material to reduce statistical scatter in the NWs´ resistance: the laser micro annealing process (LMA) for ohmic contact formation of individual NWs. Micro Raman measurements were carried out on annealed Sb_2Te_3 nanowires to monitor local degradation for the LMA process. We will demonstrate the suitability of the laser micro annealing (LMA) process and its tuning for the conditioning of individual NWs whilst focusing on their total resistance. At last the nano-optoelectronic properties of the NW hybrid device, for which the process was applied, were characterized by performing DC measurements of the dark current and the photo-responsivity.

2. Experimental

2.1. Sb_2Te_3 nanowire growth and characterization

The fabrication process started with the catalytic chemical vapor deposition (CVD) of the Sb_2Te_3 NWs [26] in a quartz tube furnace. To this end, an alumina boat with a source mixture of Sb and Te powder was placed at the center of the furnace, which was heated to 430°C for 6 hours. The Si substrate was placed 10 cm downstream of the source powder. The Si template was etched in buffered oxide etch (BOE) solution to remove the native oxide layer, followed by a deposition of a 10 nm thick Au film which served as the catalyst. Sb_2Te_3 NWs grown reached lengths between ~ 5 µm and ~ 60 µm. The morphology of the nanowires was investigated on the one hand with a Hitachi S-4800 field-emission scanning electron microscope (FE-SEM) at 1kV accelerating voltage and on the other hand with a Veeco Dimension 3100 atomic force microscope (AFM) operated in tapping mode. Fig. 1 presents an SEM image as well as an AFM scan of a typical Sb_2Te_3 nanowire exhibiting a length of ~ 5 µm and height of ~ 60 nm. The nanowires crystallize in the trigonal crystal system in the

space group R-3m [27-29] in a layered structure. The structure is characterized by quintuples of alternating Sb and Te layers. The unit cell contains three quintuples which are bonded by van der Waals interactions [30]. The structural characterization was performed with a

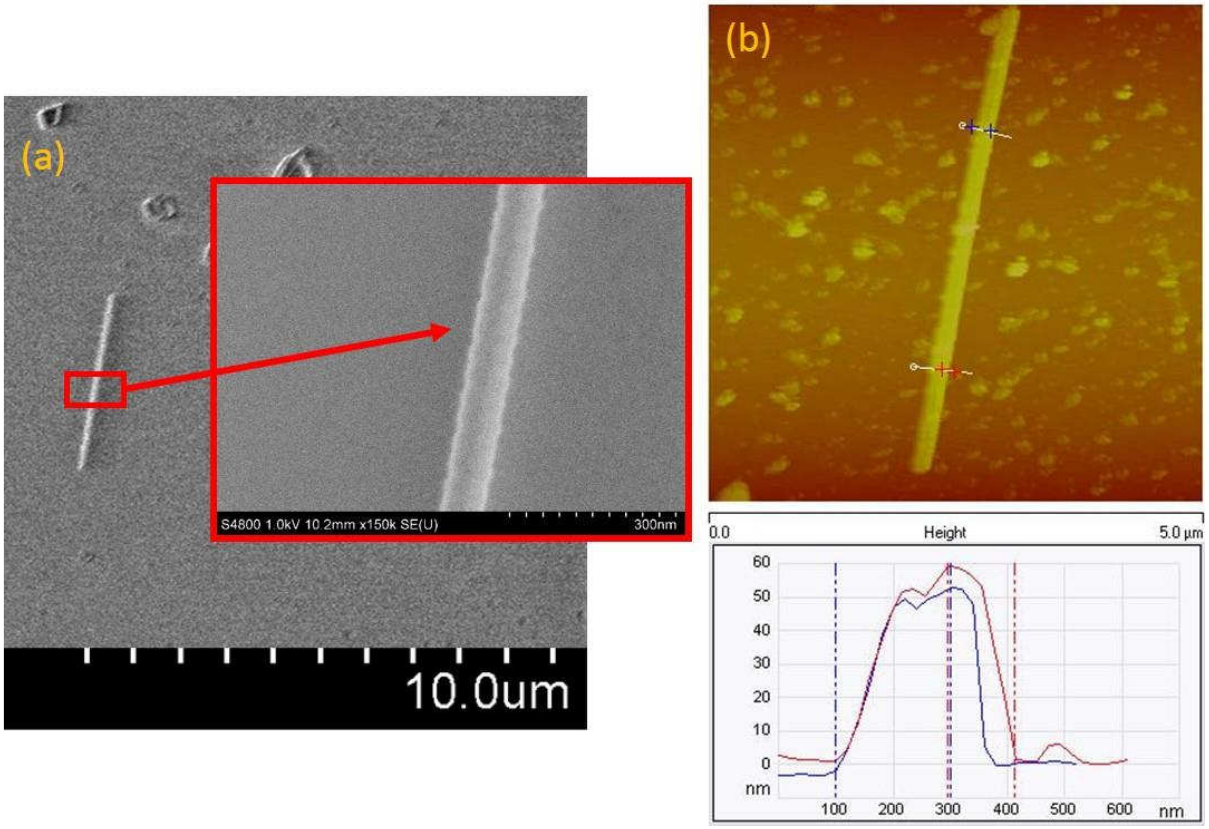

Fig. 1. a) SEM image and b) 5 µm x 5 µm AFM topography scan of a typical Sb_2Te_3 nanowire with 5µm length and 60 nm width/height.

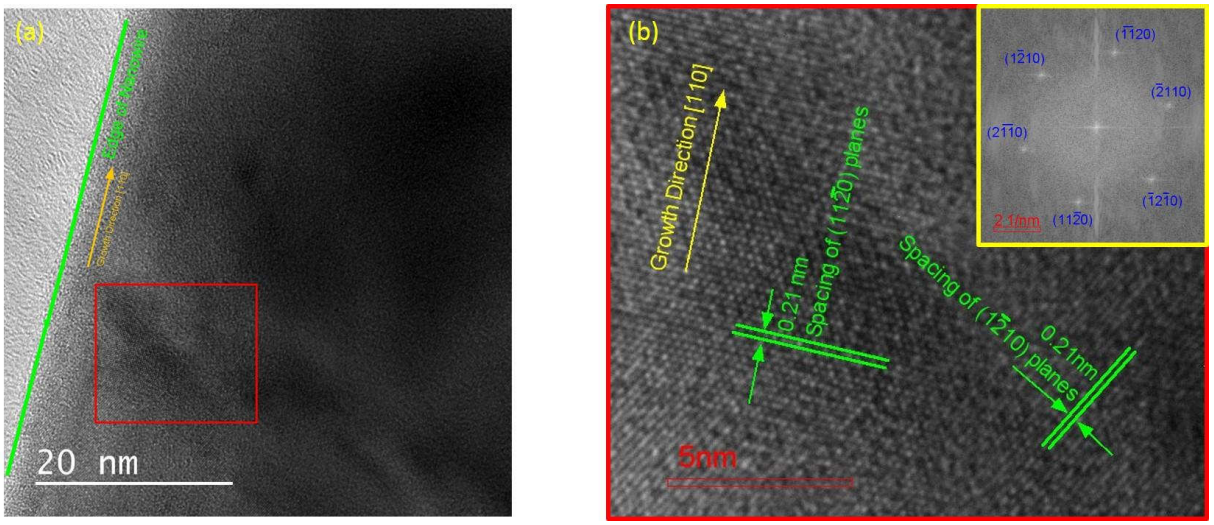

Fig. 2. a) HR-TEM image of a representative Sb_2Te_3 nanowire (top view) and b) enlarged view of the HR-TEM image indicated in a). The inset in b) presents the fast Fourier transform of the image.

transmission electron microscope (TEM) JEOL 2100 TEM/STEM operated at wide area parallel illumination mode (α = 1). A representative high resolution transmission electron microscopy image is presented in Fig.2.

2.2. Nanowire transfer, conditioning and monitoring

The Sb_2Te_3 NWs were detached from their native substrate and subsequently placed on a flexible PET (polyethylene terephthalate) substrate with the help of a quartz-glass micropipette. The procedure of nanowire transfer and positioning is shown schematically in Fig. 3.

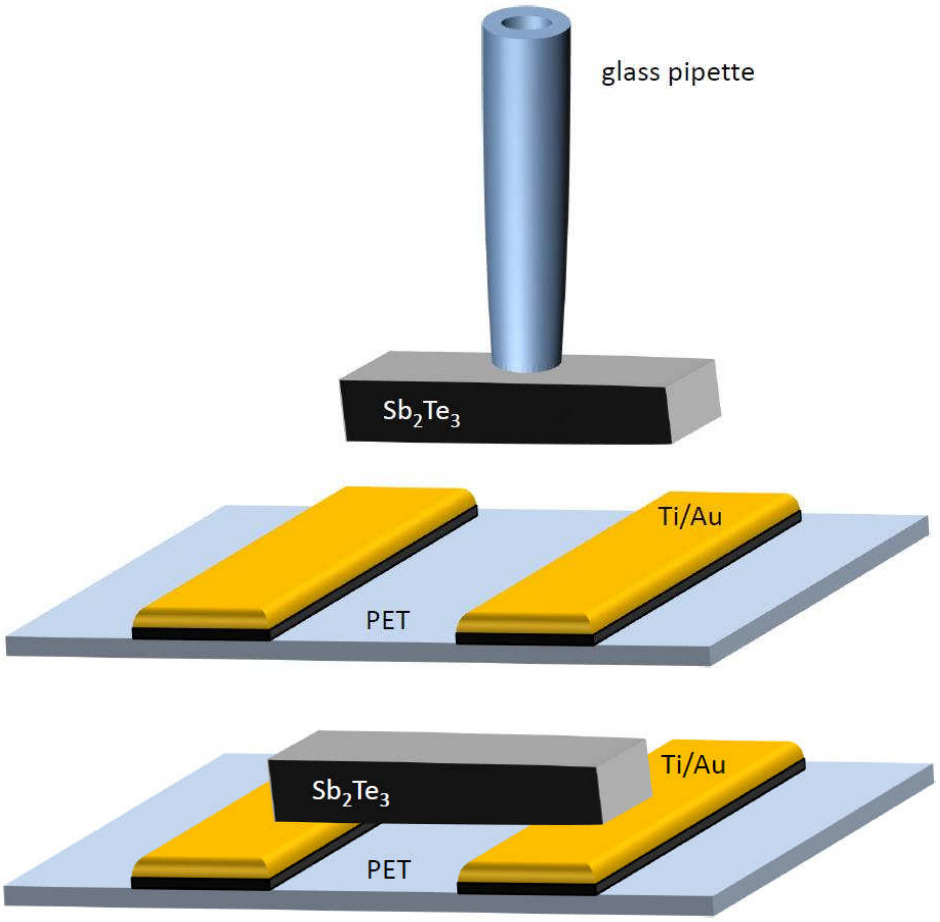

Fig. 3. Transfer and integration scheme for a freestanding Sb_2Te_3 NW prepared for nano-optoelectronic characterization as a photodetector. The NW is transferred to the host flexible PET (polyethylene terephthalate) substrate using the quartz-glass pipette/micro manipulator assisted transfer technique.

In accordance with our fabrication processes [23-25] described earlier, we employed a micrometer-sized, quartz-glass pipette for precise manipulation and transfer of our NWs to the designed coplanar strip (CPS) lines. The structure was annealed with the help of a 325 nm focused continuous wave (cw) HeCd laser beam and the power was kept constant at ~ 0.3 kW/cm^2. The aim was to improve the electrical contact and mechanical stability as well as crystallinity of the transferred Sb_2Te_3 NWs and to eliminate possible defects on their sidewalls. The laser micro annealing (LMA) procedure is shown schematically in Fig. 4.

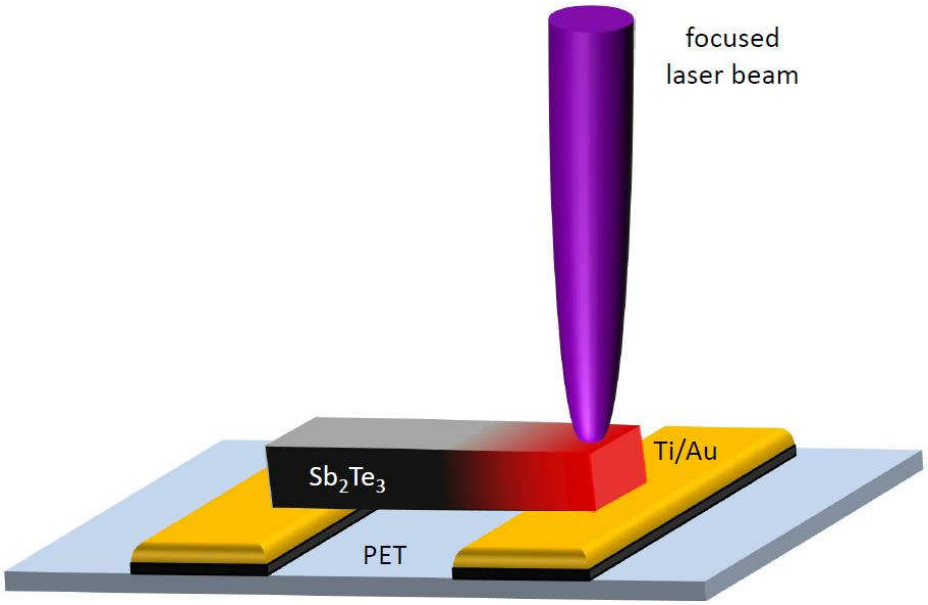

Fig. 4. Schematics of the so-called laser micro annealing (LMA) process. Precise local annealing of the NW is carried out above the Ti/Au coplanar strip line in order to achieve low resistance Sb_2Te_3/Au ohmic contacts.

Micro Raman studies were carried out on freestanding Sb_2Te_3 nanowires before and after partial annealing steps to monitor local degradation. To this end annealing was interrupted systematically and the spectra recorded. They were collected in backscattering geometry using a Renishaw inVia FSM-REFLEX confocal Raman spectrometer coupled with a 532 nm cw Nd:YAG laser. The spectra were recorded in the range from ~ 80 cm^{-1} to ~ 200 cm^{-1}. Measurements were performed at several points between the contact/coplanar strip (CPS) line area as well as at the annealed contact area at the nanowire surface with an acquisition time of 10 s. The excitation power was determined to be ~ 0.1 mW which provided an acceptable signal/noise ratio without phase-change initialization or damaging of freestanding nanowires.

2.2 device characterization

After the laser annealing process (Fig. 5.), the Sb_2Te_3 nanowire structures were first tested by DC measurements in the dark and under continuous wave 1550 nm illumination with a laser light input power of 180 µW. It should be noted that the laser beam was focused onto an area (~ 5 µm in diameter) between the coplanar strip lines. The resistance of the NWs integrated into coplanar strip lines was subsequently determined at a fixed bias voltage of 100 mV as a function of the total annealing time - i.e. annealing was interrupted systematically and the resistance data collected. The results of six representative NWs are presented.

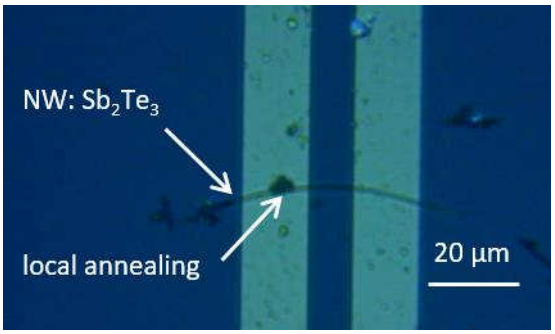

Fig. 5. Micrograph of a Sb_2Te_3 NW integrated in coplanar strip (CPS) lines. The NW is transferred to the host flexible PET (polyethylene terephthalate) substrate.

3. Results

Fig. 6 presents the resistance of a Sb_2Te_3 nanowire as a function of the annealing time. Each data point was obtained by carrying out dark current and photocurrent measurements and calculating the resistance as presented in Fig. 7. In the following four different regions were identified. At first, the resistance decreases with the annealing time very strongly by many orders of magnitude. As the total annealing time increases further, the slope of the resistance curve becomes less steep. In this second region, the resistance decreases only very gradually with time and reaches its lowest values of ~ 1.0-1.2 kΩ/µm. In region III, the resistance increases very strongly until it reaches values in the ~ GΩ range in region IV indicative of the NWs´ decomposition stage. This was confirmed also by optical inspection.

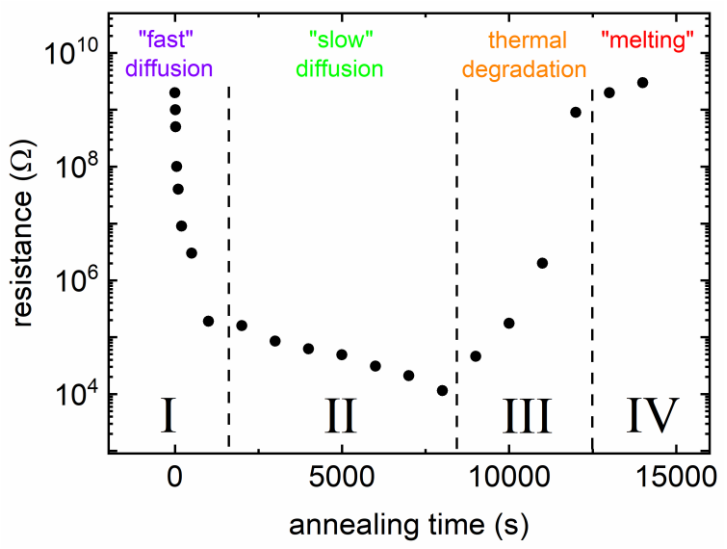

Fig. 6. Resistance at a fixed bias of 100 mV as a function of the total annealing time (LMA process, constant input HeCd laser power ~ 0.3 kW/cm^2) for a Sb_2Te_3 NW integrated into coplanar strip (CPS) lines. Empirically, four different regions are found.

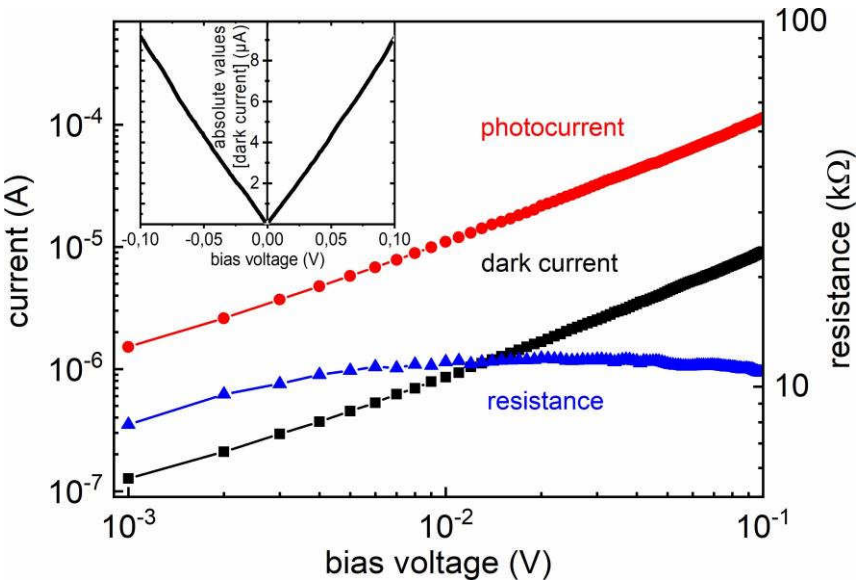

Fig. 7. Dark current and calculated resistance as well as photocurrent (at 1550 nm illumination and optical power of ~180 μW) measurements of a single Sb_2Te_3 nanowire integrated in coplanar strip (CPS) lines. Inset presents absolute values of dark current for negative and positive bias voltage range demonstrating nearly symmetrical behavior of the current-voltage characteristics for both regions.

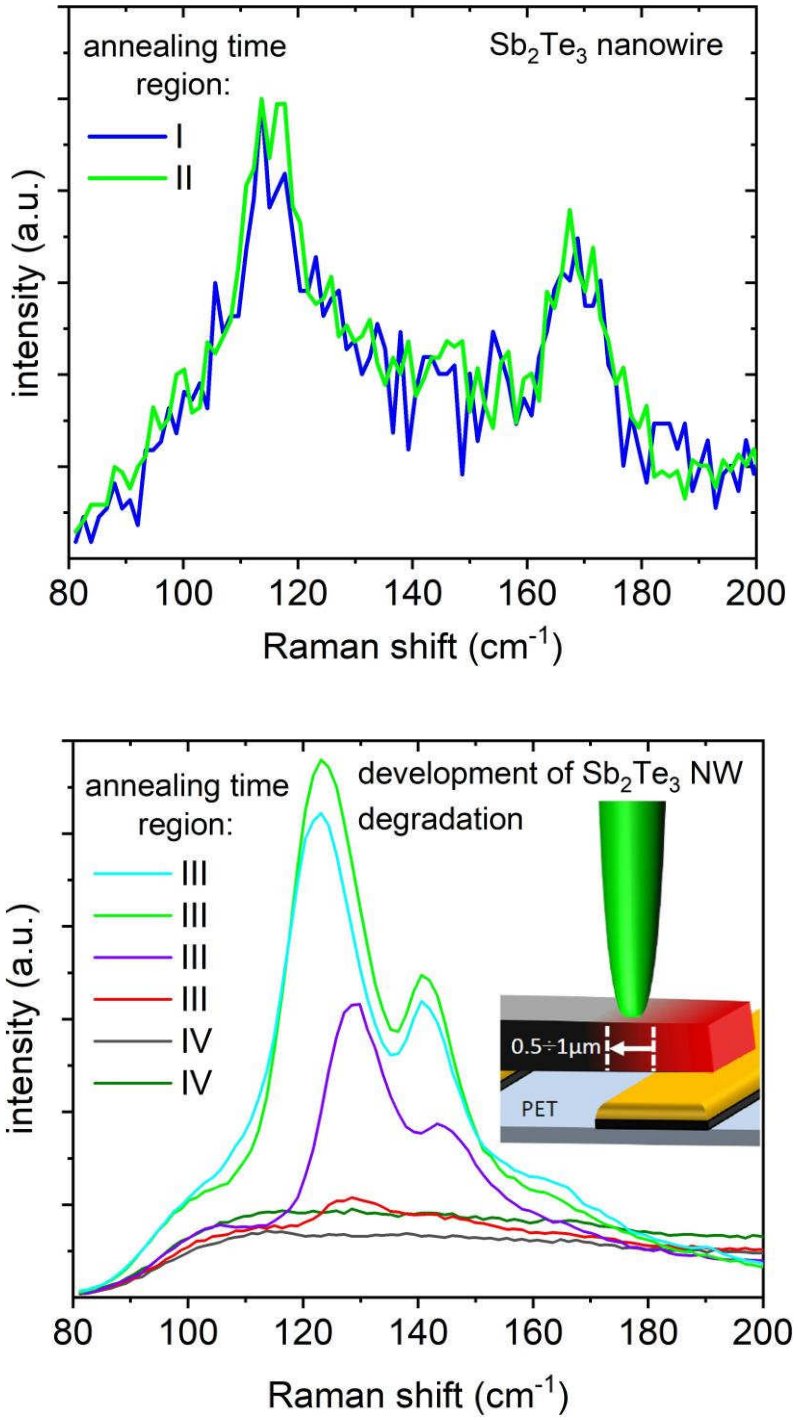

Fig. 8. Representative micro Raman spectra recorded at ~ 500 nm÷1000 nm inner length of the NWs. For annealing time regions (I and II) - no evidence for structural degradation processes in the active central NW´s area was found (top) and a development of Sb_2Te_3 nanowire degradation was observed for annealing time regions III and IV (bottom).

Complementary Raman studies were carried out on different areas of the NWs between the CPS lines / contact regions. For the sake of comparability, spectra recorded at ~ 500 nm÷1000 nm inner length of the NWs from the contact area (see inset) are presented in

Fig. 8. Representative spectra recorded in the annealing region I and II are depicted in Fig. 8 top. The spectra are similar and comparable to intrinsic NWs (not shown here) and exhibit two bands related to vibrations in crystalline Sb_2Te_3 at ~ 117 cm^{-1} and at ~ 170 cm^{-1}. They are attributed to the E^2_g and A^2_{1g} modes of the Sb-Te vibrations, respectively, and are consistent with data previously presented [31-35] for crystalline Sb_2Te_3. The Raman spectra remain unchanged until the annealing time reaches the region III. Upon further annealing, a deterioration is detectable in the Raman spectra and that within the first ~ 500 nm÷1000 nm inner length of both sides of the NWs. Figure 8 (bottom) presents the evolution of Raman spectra from the annealing region III towards the region IV.

A broadening of all active Raman peaks is observed indicative of the onset of defect formation [36], phase change (amorphization) and disorder [37] and at last decomposition. The Raman spectra exhibit an additional peak at around 140 cm^{-1} which is not associated with vibrations in Sb_2Te_3. A comparison to spectra reported for other possible materials, which could develop upon annealing such as elemental antimony, elemental tellurium, Sb_2O_3 and TeO_2 reveals, that this peak can be attributed to Te-Te vibrations [38,39]. It indicates that the original nanowire material changes, Te accumulates and segregates within the material and the stoichiometric composition is no longer homogeneous.

Current-voltage measurements performed on annealed Sb_2Te_3 nanowire structures exhibit ~ ohmic dependence up to ~ 100 mV. Similarly, their photocurrent shows also the same dependence in the whole measured bias range. The absolute values of dark current for the negative and positive bias voltage range exhibit nearly symmetrical behavior of the current-voltage characteristics for both regions. Fig. 7 and its inset present this behavior exemplarily for one of the nanowires annealed with the LMA process using an annealing time in region II, in which we achieved the lowest resistance with the LMA process. Low dark currents below 10^{-5}A at 100 mV bias as well as high DC photo-responsivity ~ 0.6 A/W were achieved. These nanowire devices are very promising candidates for highly sensitive infrared optoelectronic devices such as sensors and photodetectors.

Resistance values determined for six representative different NWs integrated into coplanar strip lines are presented in an overview diagram in Fig. 9 as a function of total annealing time. The resistance values are compared at a fixed bias of 100 mV as a function of annealing time in the LMA process using a constant input laser power ~ 0.3 kW/cm^2. The resistance vs. annealing time characteristics follow nearly identical behavior for all NWs in the series within a very narrow range: 4 different basic annealing time regions are found empirically similar to those presented in Fig. 6. The results demonstrate that this observation

is a feature of the LMA process for Sb_2Te_3 NWs. The lower diagram presents a detailed view of the annealing time region in which the minimum resistance values are achieved. The resistance of every individual nanowire can be tuned to the mutual minimum resistance value detected for all the NWs by applying the appropriate annealing time. A suppression of statistical scatter in the nanowire´s resistance after applying the time dependent and time adjusted annealing process is demonstrated therefore for six representative NWs.

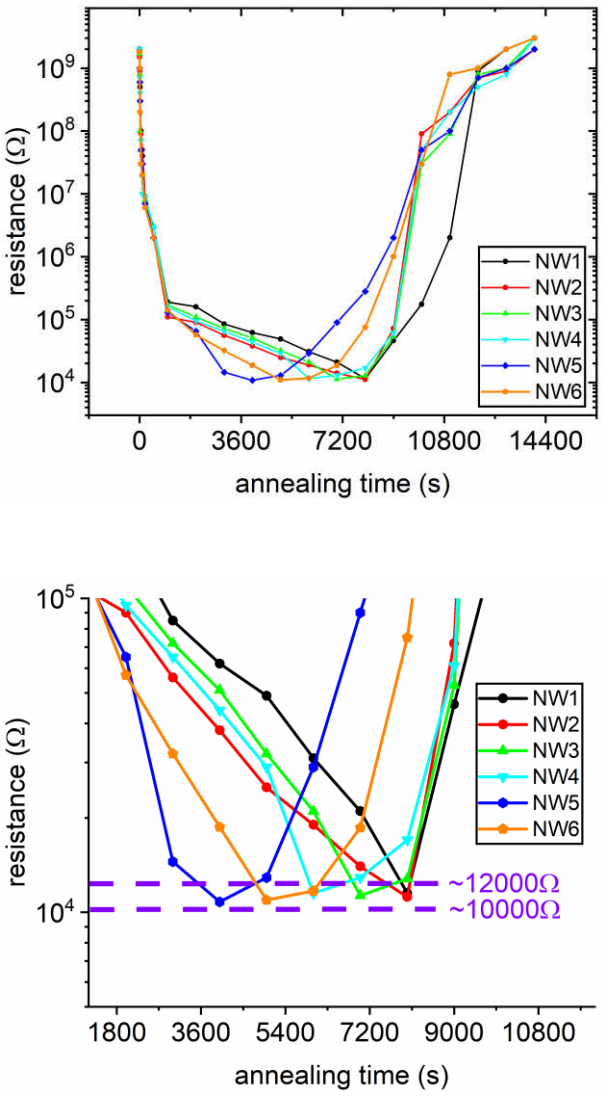

Fig. 9. Comparison of resistance values at a fixed bias of 100 mV as a function of annealing time (LMA process, constant input HeCd laser power ~ 0.3 kW/cm^2) for 6 representative nanowire structures integrated into coplanar strip (CPS) lines (top) and detail from measured characteristics (bottom): the suppression of statistical scatter in nanowire´s resistance after "time dependent/adjusted" annealing process is demonstrated for all 6 NWs.

4. Discussion

The formation of ohmic contacts to semiconductors is governed by an alloying process. After choosing an appropriate metal as a low resistance contact for alloying, conditions need to be found at which the alloying can take place. The alloy formation occurs by diffusion into the semiconductor. To this end, thermal energy is applied by an annealing process. The disadvantage is, however, that the annealing process cannot be carried out locally and the whole (nano-) structure must withhold the thermal treatment [40]. The treatment must avoid any melting or deterioration of the whole nano-structure, which is a challenge for the highly sensitive layered material family such as for Sb_2Te_3. For the latter the temperature must stay well below its melting temperature (616°C [41], the melting point is reported to be even lower for low dimensional structures [42]).

The advantage of the laser micro annealing process is, that energy is transferred by a focused laser beam locally to the part of the device in which the contact formation is desired: the nanowire part situated directly above Ti/Au coplanar strip lines. Since the contact metal Au forms a eutectic point with Sb as well as with Te at 447°C and 360°C, respectively [43-45], these characteristics can be utilized for contact formation. (Also, due to these characteristics, the nanowires can be deposited by the vapor liquid solid (VLS) method using Au particles [26], as described above for the nanowires employed here). Gold is well-known for its rather fast diffusion in materials during contact formation [46,47]. Preferentially it diffuses by an interstitial/substitutional mechanism through the lattice and needs therefore vacancies. Layered materials such as crystalline Sb_2Te_3, which exhibit van der Waals gaps, are therefore especially prone to such diffusion via their gaps [48]. As the laser locally heats up the nanowires further, the eutectic points are reached. At this point, the onset of strong diffusion will occur in the annealing process. Due to the high chemical potential difference at the interface between the Au of coplanar strip lines and the Sb_2Te_3 NW interface, the diffusion will be faster at first. However, as the solubility limit is approached, the diffusion will slow down. The decrease in resistance in regions I + II is therefore most probably related to the fast diffusion process of Au into the Sb_2Te_3 NW at first and a subsequent slower diffusion process thereafter. In region III thermal effects start to dominate the resistance behavior and the degradation of the NW sets in as confirmed by micro Raman measurements presented in Fig. 8 (bottom). The resistance increases strongly. In region IV, after ~ 3.5 hours, the total resistance reaches values up to ~ GΩ range and the NWs start to melt and to decompose. The study of the resistance vs. annealing time for different NWs from the same

series reveals, that the characteristics follow nearly identical behavior for all NWs in the series (Fig. 9) within a very narrow range: they all exhibit the 4 different basic regions - a “fast” and “slow” diffusion as well as a “thermal degradation” and a “melting” region – similar to those presented in Fig. 6.

The origin of the different nanowire resistance values could be attributed to statistical processes initialized as a consequence of fluctuations. They could be caused by the NW´s growth and probably more dominantly by the formation of defects during the NW separation and transfer procedure from the native i.e. ”mother” substrate to the coplanar strip lines. Additionally, surface corrosion reactions - especially oxidation – induced by the “reactive” environmental conditions affect directly the surface states and will influence ohmic contact formation as well. A passivation of surfaces is the conventional way to prevent such degradation processes. However, the intentionally un-passivated and non-annealed Sb_2Te_3 NWs studied here did not exhibit any significant changes in their properties in the time range of the investigation. In our study, we centered our attention to the evaluation of the intrinsic Sb_2Te_3 nanowire properties and endeavored to eliminate any possible influence of additional passivation layers on their properties. Therefore, only structures prepared under the same fabrication conditions were used for conditioning the NWs by laser micro annealing. It is evident that a careful adjustment of the annealing time leads to a reduction of nanowire`s resistance by many orders of magnitude to ~11 kΩ. Furthermore, the resistance is within a ±10% range of this value for ~ 90% of the NW structures. This indicates that our process is a powerful procedure and effectively suppresses statistical scatter in nanowire resistance even for such highly sensitive layered NW materials as Sb_2Te_3. In addition, the LMA process provides new prospects in the integration of a large amount of NWs in highly sophisticated computational units and circuits. A further optimization of the laser annealing process with respect to a precise tuning of the laser power density and annealing time in combination with device monitoring in short time intervals could be beneficial to the additional decrease in scatter in the NW´s minimum resistance values to the low “few” percentage range. A deeper investigation into the mechanism behind the formation of Au contacts to Sb_2Te_3 NWs as well as behind the reduction of statistical scatter in NW resistance will be in the scope of our future work.

5. Conclusions

In conclusion, a highly efficient transfer and integration technology was introduced for freestanding Sb_2Te_3 NWs. They were integrated into coplanar strip lines on flexible PET substrates suitable for nano-optoelectronic characterization. The influence of laser micro annealing on resistance was investigated and the annealing procedure optimized. This process was individually adjusted also for a series of NWs fabricated from the same Sb_2Te_3 nanowire deposition run resulting in the suppression of statistical scatter: a relatively narrow range around the average nanowire resistance is achieved. Low dark currents below 10^{-5}A at 100 mV bias as well as high DC photo-responsivity ~ 0.6 A/W were accomplished. The nanowire devices conditioned by laser micro annealing are very promising candidates for highly sensitive infrared optoelectronic applications.

Acknowledgement

J. Z. Zhang thanks the Office of China Postdoc Council (OCPC) and the Forschungszentrum Jülich GmbH for jointly funding his two year fellowship within the Jülich-OCPC-Programme for the involvement of postdocs in bilateral collaboration projects.

References

[1] F. Zoller, K. Peters, P.M. Zehetmaier, P. Zeller, M. Döblinger, T. Bein, et al., Making Ultrafast High-Capacity Anodes for Lithium-Ion Batteries via Antimony Doping of Nanosized Tin Oxide/Graphene Composites, Adv. Funct. Mater. 28 (2018) 1706529. doi:10.1002/adfm.201706529.

[2] C.C. Mayorga-Martinez, R. Gusmão, Z. Sofer, M. Pumera, Pnictogen-Based Enzymatic Phenol Biosensors: Phosphorene, Arsenene, Antimonene, and Bismuthene, Angew. Chemie Int. Ed. 58 (2019) 134–138. doi:10.1002/anie.201808846.

[3] B. Khezri, S.M. Beladi Mousavi, L. Krejčová, Z. Heger, Z. Sofer, M. Pumera, Ultrafast Electrochemical Trigger Drug Delivery Mechanism for Nanographene Micromachines, Adv. Funct. Mater. 29 (2019) 1806696. doi:10.1002/adfm.201806696.

[4] R. Gusmão, Z. Sofer, M. Pumera, Exfoliated Layered Manganese Trichalcogenide Phosphite (MnP X 3 , X = S, Se) as Electrocatalytic van der Waals Materials for Hydrogen Evolution, Adv. Funct. Mater. 29 (2019) 1805975. doi:10.1002/adfm.201805975.

[5] Y. Li, F. Qian, J. Xiang, C.M. Lieber, Nanowire electronic and optoelectronic devices, Mater. Today. 9 (2006) 18–27. https://doi.org/10.1016/S1369-7021(06)71650-9.
[6] V.M. Agranovich, Y.N. Gartstein, M. Litinskaya, Hybrid Resonant Organic–Inorganic Nanostructures for Optoelectronic Applications, Chem. Rev. 111 (2011) 5179–5214. https://doi.org/10.1021/cr100156x.
[7] R. Calarco, M. Marso, T. Richter, A.I. Aykanat, R. Meijers, A. v.d. Hart, et al., Size-dependent Photoconductivity in MBE-Grown GaN−Nanowires, Nano Lett. 5 (2005) 981–984. https://doi.org/10.1021/nl0500306.
[8] Y. Wang, X. Wang, B. Zhu, Z. Shi, J. Yuan, X. Gao, et al., Full-duplex light communication with a monolithic multicomponent system, Light Sci. Appl. 7 (2018) 83. https://doi.org/10.1038/s41377-018-0083-0.
[9] C. Qin, X. Gao, J. Yuan, Z. Shi, Y. Jiang, Y. Liu, et al., Transferrable monolithic multicomponent system for near-ultraviolet optoelectronics, Appl. Phys. Express. 11 (2018) 051201. https://doi.org/10.7567/APEX.11.051201.
[10] Y. Robin, Y. Liao, M. Pristovsek, H. Amano, Simultaneous Growth of Various InGaN/GaN Core-Shell Microstructures for Color Tunable Device Applications, Phys. Status Solidi. 215 (2018) 1800361. doi:10.1002/pssa.201800361.
[11] H. Hardtdegen, M. Mikulics, Towards III-nitride nano-LED based single photon emitters: Technology and applications, in: 2016 11th Int. Conf. Adv. Semicond. Devices Microsystems, IEEE, 2016: pp. 27–32. https://doi.org/10.1109/ASDAM.2016.7805887.
[12] M. Mikulics, Y.C. Arango, A. Winden, R. Adam, A. Hardtdegen, D. Grützmacher, et al., Direct electro-optical pumping for hybrid CdSe nanocrystal/III-nitride based nano-light-emitting diodes, Appl. Phys. Lett. 108 (2016) 061107. https://doi.org/10.1063/1.4941923.
[13] S. Heedt, C. Morgan, K. Weis, D.E. Bürgler, R. Calarco, H. Hardtdegen, et al., Electrical Spin Injection into InN Semiconductor Nanowires, Nano Lett. 12 (2012) 4437–4443. https://doi.org/10.1021/nl301052g.
[14] V.A. Guzenko, J. Knobbe, H. Hardtdegen, T. Schäpers, A. Bringer, Rashba effect in InGaAs⁄InP parallel quantum wires, Appl. Phys. Lett. 88 (2006) 032102. https://doi.org/10.1063/1.2165279.
[15] T. Schäpers, C. Weyrich, D. Rosenbach, J. Kölzer, P. Schüffelgen, G. Mussler, et al., Phase-coherent transport in topological insulator nanocolumns and nanoribbons, in: H. Jaffrès, H.-J. Drouhin, J.-E. Wegrowe, M. Razeghi (Eds.), Spintron. XI, SPIE, 2018: p. 30. https://doi.org/10.1117/12.2322720.
[16] R.T. Young, C.W. White, G.J. Clark, J. Narayan, W.H. Christie, M. Murakami, et al.,

Laser annealing of boron-implanted silicon, Appl. Phys. Lett. 32 (1978) 139–141. doi:10.1063/1.89959.
[17] P. Baeri, S.U. Campisano, G. Foti, E. Rimini, A melting model for pulsing-laser annealing of implanted semiconductors, J. Appl. Phys. 50 (1979) 788–797. doi:10.1063/1.326046.
[18] G.K. Celler, J.M. Poate, L.C. Kimerling, Spatially controlled crystal regrowth of ion-implanted silicon by laser irradiation, Appl. Phys. Lett. 32 (1978) 464–466. doi:10.1063/1.90109.
[19] C. Lee, P. Srisungsitthisunti, S. Park, S. Kim, X. Xu, K. Roy, et al., Control of Current Saturation and Threshold Voltage Shift in Indium Oxide Nanowire Transistors with Femtosecond Laser Annealing, ACS Nano. 5 (2011) 1095–1101. doi:10.1021/nn102723w.
[20] S. Kim, S. Kim, P. Srisungsitthisunti, C. Lee, M. Xu, P.D. Ye, M. Qi, X. Xu, C. Zhou, S. Ju, D.B. Janes, Selective Contact Anneal Effects on Indium Oxide Nanowire Transistors using Femtosecond Laser, J. Phys. Chem. C. 115 (2011) 17147–17153. https://doi.org/10.1021/jp203342j.
[21] H. Kwon, W. Choi, D. Lee, Y. Lee, J. Kwon, B. Yoo, et al., Selective and localized laser annealing effect for high-performance flexible multilayer MoS_2 thin-film transistors, Nano Res. 7 (2014) 1137–1145. doi:10.1007/s12274-014-0476-1.
[22] J. Ha, B.J. Lee, D.J. Hwang, D. Kim, Femtosecond laser nanowelding of silver nanowires for transparent conductive electrodes, RSC Adv. 6 (2016) 86232–86239. doi:10.1039/C6RA19608J.
[23] M. Mikulics, J. Zhang, J. Serafini, R. Adam, D. Grützmacher, R. Sobolewski, Subpicosecond electron-hole recombination time and terahertz-bandwidth photoresponse in freestanding GaAs epitaxial mesoscopic structures, Appl. Phys. Lett. 101 (2012) 031111. https://doi.org/10.1063/1.4737442.
[24] M. Mikulics, H. Hardtdegen, R. Adam, D. Grützmacher, D. Gregušová, J. Novák, et al., Impact of thermal annealing on nonequilibrium carrier dynamics in single-crystal, freestanding GaAs mesostructures, Semicond. Sci. Technol. 29 (2014) 045022. https://doi.org/10.1088/0268-1242/29/4/045022.
[25] M. Mikulics, M. Marso, R. Adam, M. Schuck, A. Fox, R. Sobolewski, et al., Electrical and optical characterization of freestanding $Ge_1Sb_2Te_4$ nano-membranes integrated in coplanar strip lines, in: 2016 11th Int. Conf. Adv. Semicond. Devices Microsystems, IEEE, 2016: pp. 73–76. https://doi.org/10.1109/ASDAM.2016.7805898.
[26] J.S. Lee, S. Brittman, D. Yu, H. Park, Vapor–Liquid–Solid and Vapor–Solid Growth of

Phase-Change Sb_2Te_3 Nanowires and Sb_2Te_3 / GeTe Nanowire Heterostructures, J. Am. Chem. Soc. 130 (2008) 6252–6258. doi:10.1021/ja711481b.
[27] S.A. Semiletov, No Title, Sov. Phys. Crystallogr. 1 (1956) 317–319.
[28] T.L. Anderson, H.B. Krause, Refinement of the Sb_2Te_3 and Sb_2Te_2Se structures and their relationship to nonstoichiometric $Sb_2Te_{3-y}Se_y$ compounds, Acta Crystallogr. Sect. B Struct. Crystallogr. Cryst. Chem. 30 (1974) 1307–1310. doi:10.1107/S0567740874004729.
[29] O.G. Karpinsky, L.E. Shelimova, M.A. Kretova, An X-ray study of the mixed-layered compounds of $(GeTe)_n$ $(Sb_2Te_3)_m$ homologous series, J. Alloys Compd. 268 (1998) 112–117. doi: 10.1016/S0925-8388(97)00625-7.
[30] T.L. Anderson, H.B. Krause, Refinement of the Sb_2Te_3 and Sb_2Te_2Se structures and their relationship to nonstoichiometric Sb 2 Te 3− y Se y compounds, Acta Crystallogr. Sect. B Struct. Crystallogr. Cryst. Chem. 30 (1974) 1307–1310. https://doi.org/10.1107/S0567740874004729.
[31] G. Hao, X. Qi, Y. Fan, L. Xue, X. Peng, X. Wei, J. Zhong, Spiral growth of topological insulator Sb_2Te_3 nanoplates, Appl. Phys. Lett. 102 (2013) 013105. https://doi.org/10.1063/1.4773587.
[32] K.A. Kokh, V.V. Atuchin, T.A. Gavrilova, N.V. Kuratieva, N.V. Pervukhina, N.V. Surovtsev, Microstructural and vibrational properties of PVT grown Sb_2Te_3 crystals, Solid State Commun. 177 (2014) 16–19. https://doi.org/10.1016/j.ssc.2013.09.016.
[33] K.M.F. Shahil, M.Z. Hossain, V. Goyal, A.A. Balandin, Micro-Raman spectroscopy of mechanically exfoliated few-quintuple layers of Bi_2Te_3, Bi_2Se_3, and Sb_2Te_3 materials, J. Appl. Phys. 111 (2012) 054305. https://doi.org/10.1063/1.3690913.
[34] G.C. Sosso, S. Caravati, M. Bernasconi, Vibrational properties of crystalline Sb_2Te_3 from first principles, J. Phys. Condens. Matter. 21 (2009) 095410. https://doi.org/10.1088/0953-8984/21/9/095410.
[35] W. Richter, C.R. Becker, A Raman and far-infrared investigation of phonons in the rhombohedral V2–VI3 compounds Bi_2Te_3, Bi_2Se_3, Sb_2Te_3 and $Bi_2(Te_{1-x}Se_x)_3$ ($0 < x < 1$), $(Bi_{1-y}Sb_y)_2Te_3$ ($0 < y < 1$), Phys. Status Solidi. 84 (1977) 619–628. https://doi.org/10.1002/pssb.2220840226.
[36] G. Lucazeau, Effect of pressure and temperature on Raman spectra of solids: anharmonicity, J. Raman Spectrosc. 34 (2003) 478–496. https://doi.org/10.1002/jrs.1027.
[37] H. Choi, S. Jung, T.H. Kim, J. Chae, H. Park, K. Jeong, J. Park, M.-H. Cho, Enhancement of carrier lifetime by spin–orbit coupling in a topological insulator of an Sb_2Te_3 thin film, Nanoscale. 8 (2016) 19025–19035. https://doi.org/10.1039/C6NR05852C.

[38] B.H. Torrie, Raman spectrum of tellurium, Solid State Commun. 8 (1970) 1899–1901. https://doi.org/10.1016/0038-1098(70)90343-1.
[39] D. Das, K. Malik, A.K. Deb, S. Dhara, S. Bandyopadhyay, A. Banerjee, Defect induced structural and thermoelectric properties of Sb_2Te_3 alloy, J. Appl. Phys. 118 (2015) 045102. https://doi.org/10.1063/1.4927283.
[40] S. Wirths, M. Mikulics, P. Heintzmann, A. Winden, K. Weis, C. Volk, et al., Preparation of Ohmic contacts to GaAs/AlGaAs-core/shell-nanowires, Appl. Phys. Lett. 100 (2012) 042103. https://doi.org/10.1063/1.3678639.
[41] B. Legendre, C. Hancheng, S. Bordas, M.T. Clavaguera-Mora, Phase diagram of the ternary system Ge-Sb-Te. I. The subternary GeTe-Sb_2Te_3-Te, Thermochim. Acta. 78 (1984) 141–157. doi:10.1016/0040-6031(84)87142-7.
[42] M. Longo, Nanowire phase change memory (PCM) technologies: properties and performance, Advances in Non-Volatile Memory and Storage Technology, Woodhead Publishing-Elsevier, 2014, pp. 231–261, http://dx.doi.org/10.1533/9780857098092.2.231.
[43] H. Okamoto, T. Massalski, The Au-Te (Gold-Tellurium) System, Bull. Alloy Phase Diagrams. 5 (1984) 172–177, https://doi.org/10.1007/BF02868955.
[44] H. Yasuda, H. Mori, Phase diagrams in nanometer-sized alloy systems, J. Cryst. Growth. 239 (2002) 234–238. doi:10.1016/S0022-0248(01)01881-4.
[45] H. Hardtdegen, M. Mikulics, S. Rieß, M. Schuck, T. Saltzmann, U. Simon, et al., Modern chemical synthesis methods towards low-dimensional phase change structures in the Ge–Sb–Te material system, Prog. Cryst. Growth Charact. Mater. 61 (2015) 27–45. doi:10.1016/j.pcrysgrow.2015.10.001.
[46] U.M. Gosele, Fast Diffusion in Semiconductors, Annu. Rev. Mater. Sci. 18 (1988) 257–282. https://doi.org/10.1146/annurev.ms.18.080188.001353.
[47] E. Song, B.S. Swartzentruber, C.R. Koripella, J.A. Martinez, Highly Effective GeNi Alloy Contact Diffusion Barrier for BiSbTe Long-Term Thermal Exposure, ACS Omega. 4 (2019) 9376–9382. https://doi.org/10.1021/acsomega.9b00551.
[48] Y. Hu, G. Yang, Z. Tian, Z. Hu, Effect of annealing on the structural and thermoelectric properties of nanostructured Sb_2Te_3/Au semiconductor/metal multilayer films, J. Alloys Compd. 790 (2019) 723–731. https://doi.org/10.1016/j.jallcom.2019.03.194.